Electronic Supplementary Material (ESI) for Nanoscale.

Supporting Information

High-density growth of ultrafine PdIr nanowires on graphene: reducing the graphene wrinkles and serving as efficient bifunctional electrocatalysts for water splitting

Anzhou Yang,[ab] Tiancheng Li,[bc] Shuang Jiang,[b] Xiaoru Wang,[b] Xiaoyu Qiu,[*b] Wu Lei,[*a] and Yawen Tang[*b]

[a.] School of Chemical Engineering, Nanjing University of Science and Technology, Nanjing 210094, P. R. China. E-mail: leiwuhao@njust.edu.cn

[b.] Jiangsu Key Laboratory of New Power Batteries, Jiangsu Collaborative Innovation Center of Biomedical Functional Materials, School of Chemistry and Materials Science, Nanjing Normal University, Nanjing 210023, P. R. China. E-mail: qxy18251813615@163.com and tangyawen@njnu.edu.cn.

[c.] State Key Laboratory of Oral Diseases, West China Hospital of Stomatology, Sichuan University, Chengdu, P. R. China

Experimental section

Reagents and chemicals

Potassium tetrachloroplatinate (II) (K_2PdCl_4) and Iridium (III) chloride hydrate ($IrCl_3.xH_2O$) were purchased from Shanghai D&B biological Sci-Tech Co., Ltd. (Shanghai, China). Formaldehyde solution (HCHO) was supplied by Guangdong Guanghua Sci-Tech Co., Ltd. (Shantou, China). Poly (diallyl dimethyl ammonium chloride) (PDDA, Mw: 200000-350000) and commercial RuO_2 were purchased from Aladdin industrial corporation. (Shanghai, China). Commercial Pt/C was purchased from Shanghai Hesen Electric Co., Ltd. (Shanghai, China). All chemicals used in this study were of analytical reagent (AR) without any further purification.

Synthesis of PdIr UNWs/WFG

In a typical hydrothermal synthesis, 1 mL of 0.05M $IrCl_3$, 1 mL of 0.05M K_2PdCl_4, and 2 mL of 0.05 M PDDA were added to 9 mL deionized water solution. Then 2 mg of GO was uniformly dissolved in 2 mL DI water and added to above mixed solution. The mixture was stirred for 15 min, and then the pH value was adjusted to 12 using NaOH solution. Subsequently, 1 mL of HCHO solution (40%) was added and the mixture was transferred to a 25 mL Teflon-lined stainless-steel autoclave, heating at 120 °C for 5 h. After cooling down to room temperature, the obtained products were collected by centrifugation at 18000 rpm for 8 min, washed several times with deionized water, and then dried at 45 °C for 8 h in a vacuum dryer.

Electrochemical measurements

All electrochemical measurements were conducted using a three-electrode system on a CHI 760D electrochemical analyzer (CH Instruments, Inc., Shanghai, China) at 25 °C. The catalyst-modified glassy carbon electrode was served as the working electrode, the graphite rod was used as the auxiliary electrode, and the saturated calomel electrode was regarded as the reference electrode. The catalyst ink was prepared by dispersing 4 mg of fresh-made sample in a mixture of 0.8 mL of alcohol and 1.2 mL of deionized water via sonication for 30 min. Next, 20 μL of the catalyst ink was dropped onto the surface of the electrode. After drying, 2 μL of Nafion

solution (5 *wt*%) was coated on the surface of the modified electrode and dried again. All measurements were performed in N_2-saturated 1 M KOH aqueous electrolyte with a scan rate of 5 mV s^{-1}. The linear region of the plots were fitted using the Tafel formula Z = b log(*j*) + a, where Z referred to overpotential, *j* referred to current density, and b referred to the Tafel slope.

Characterizations

TEM and HRTEM were carried out on a JEOL JEM-2100F transmission electron microscope operated at an accelerating voltage of 200 kV. SEM images were captured on a Hitachi S-4800 scanning electron microscope, operating at the voltage of 5 kV. EDX analysis was carried out on a JEOL JSM-7600F scan electron microscopy. XRD patterns were carried out on Model D/max-rC X-ray diffractometer operated at 40 kV and 100 mA by using Cu Kα radiation source (λ= 1.5406 Å). The Raman spectra were displayed on a LabRam HR800 instrument with a green laser emitting at the wavelength of 514 nm. High-resolution XPS data were carried out on a Thermo VG Scientific ESCALAB 250 spectrometer with an Al Kα radiator and the binding energy was calibrated by means of the C 1s peak energy of 284.6 eV. UV-vis spectra were recorded on a Shimadzu UV3600 spectrophotometer equipped with an optical path length of 1 cm at room temperature.

Figures

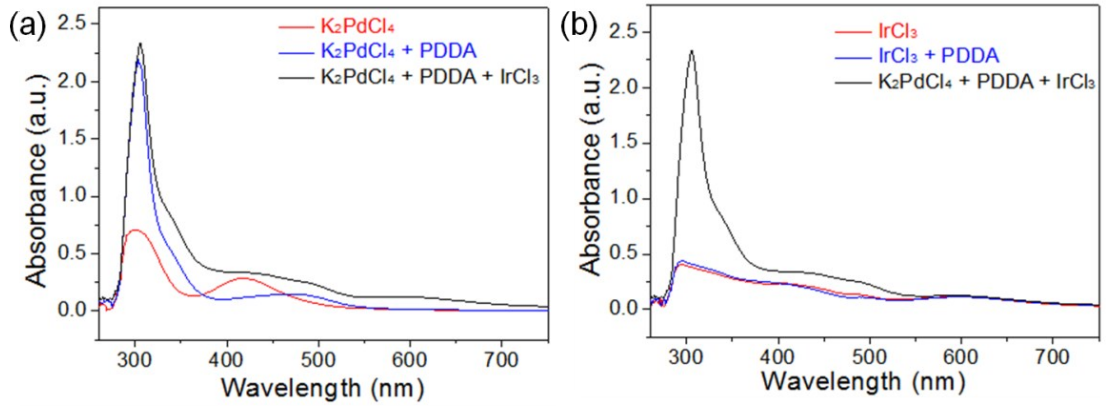

Fig. S1 (a) UV-vis spectra of K_2PdCl_4 solution (red curve), K_2PdCl_4 + PDDA solution (blue curve), and K_2PdCl_4 + PDDA + $IrCl_3$ solution (black curve). (b) UV-vis spectra of $IrCl_3$ solution (red curve), $IrCl_3$ + PDDA solution (blue curve), and $IrCl_3$+ PDDA + K_2PdCl_4 solution (black curve).

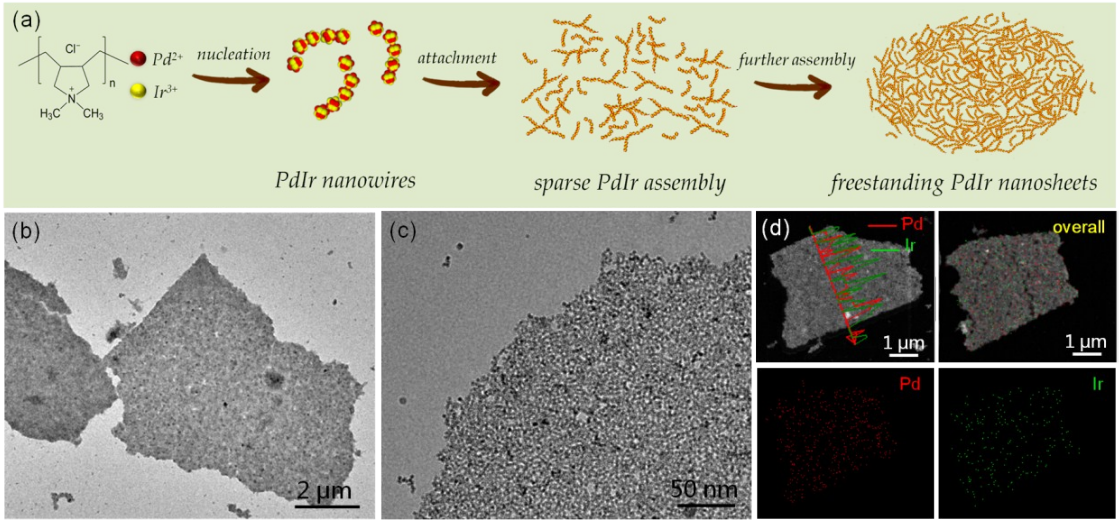

Fig. S2 Mechanism, morphological and compositional analyses of freestanding PdIr nanosheets. (a) Schematic illustration of mechanism for the formation of freestanding PdIr nanosheets, showing the particle attachment and self-assembly process. (b) TEM image, (c) amplified HRTEM image, (d) EDX line-scan profiles and elemental mapping images of freestanding PdIr nanosheets.

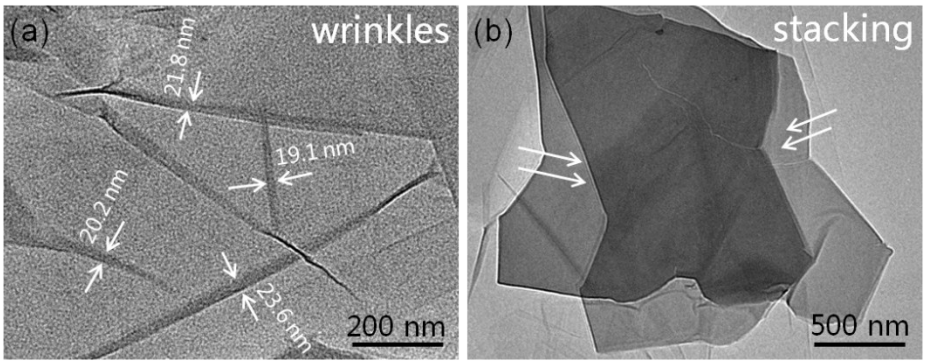

Fig. S3 Representative TEM images of (a) wrinkled graphene, (b) stacked graphene.

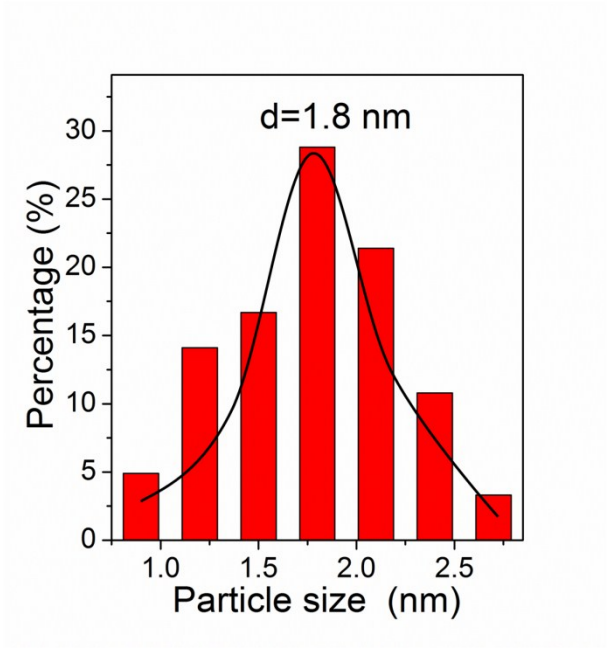

Fig. S4 Particle size distribution diagram of ultrafine PdIr nanowires on PdIr UNWs/WFG.

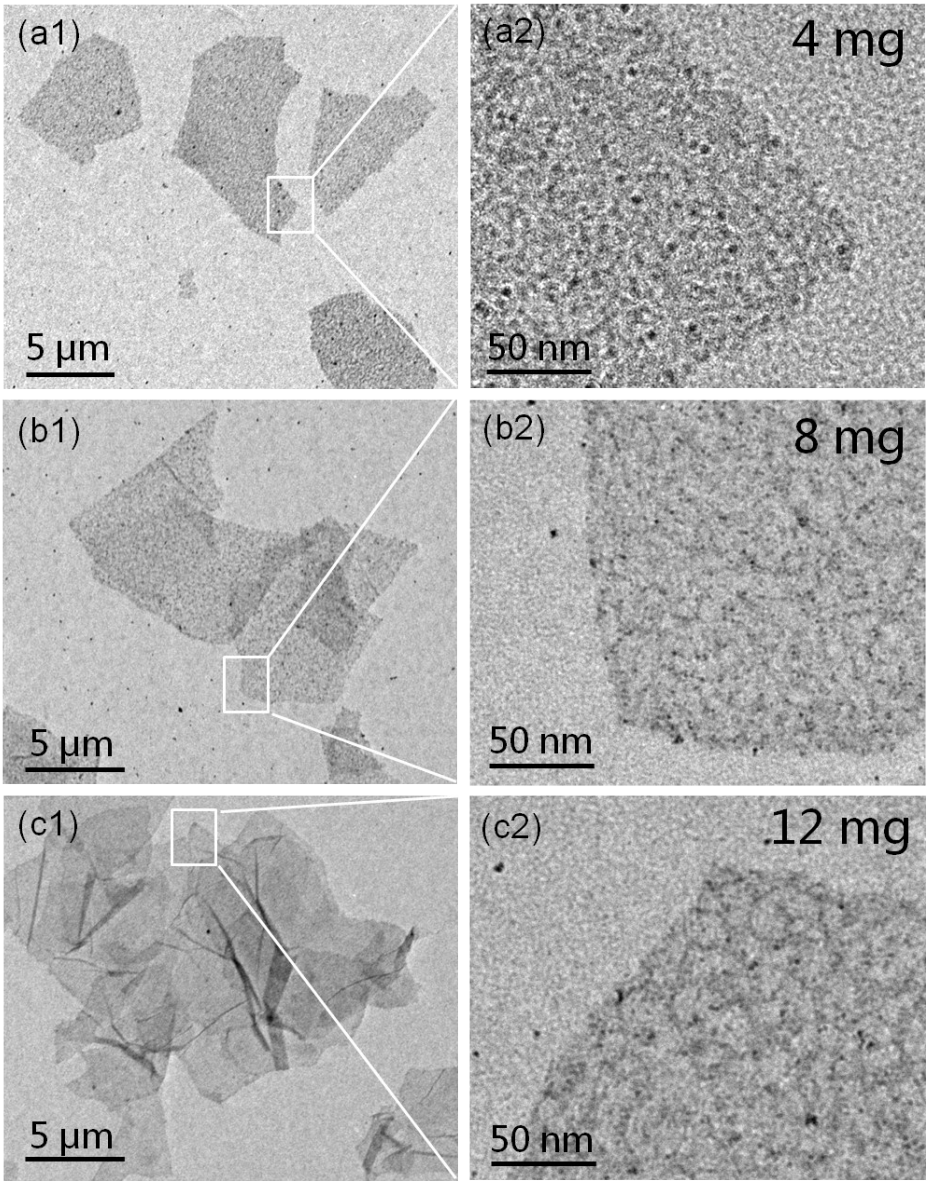

Fig. S5 Representative TEM images of products using different dosage of GO. (a1-a2) 4 mg GO, (b1-b2) 8 mg GO, (c1-c2) 12 mg GO.

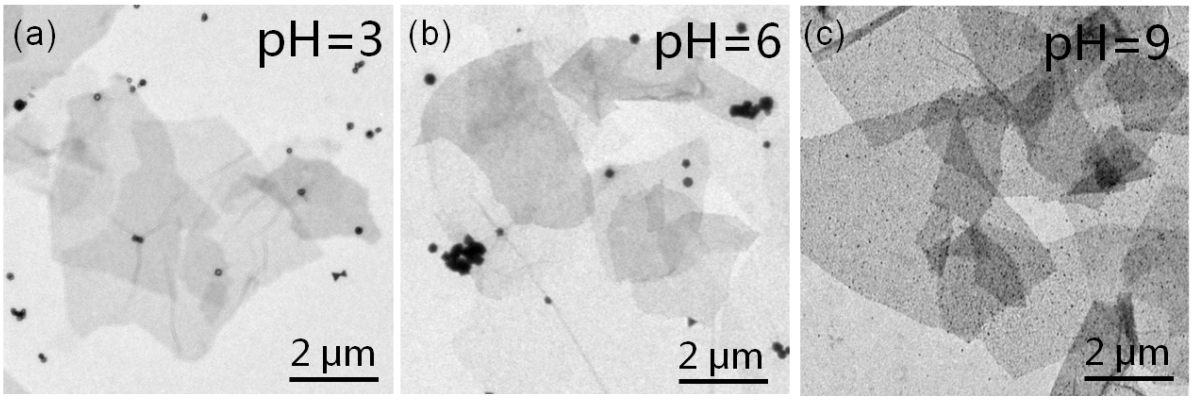

Fig. S6 Representative TEM images of products obtained at the (a) pH value of 3, (b) pH value of 6, (c) pH value of 9, respectively.

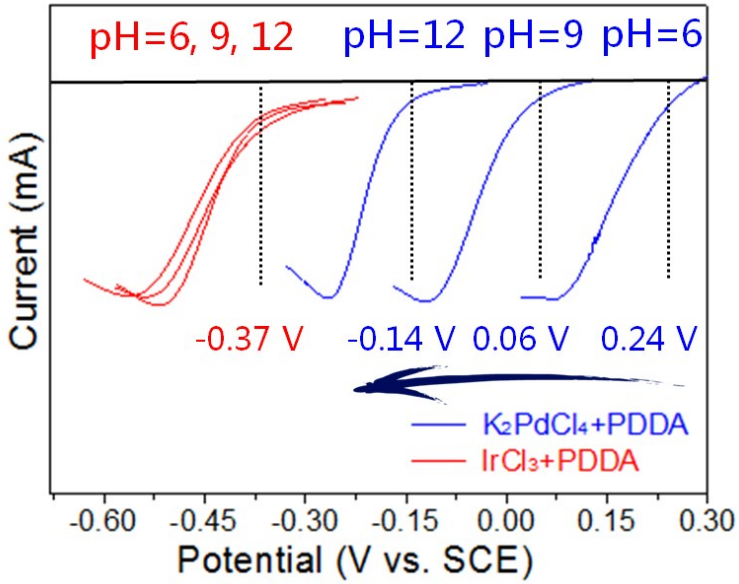

Fig. S7 Linear sweeping voltammograms of N_2-saturated 0.005 M K_2PdCl_4 + 0.01 M PDDA + 0.5 M KCl solution (blue line) and 0.005 M $IrCl_3$ + 0.01 M PDDA + 0.5 M KCl solution (red line) at the glassy carbon electrode at a pH value of 3,6,9, respectively. Scan rate: 100 mV s^{-1}.

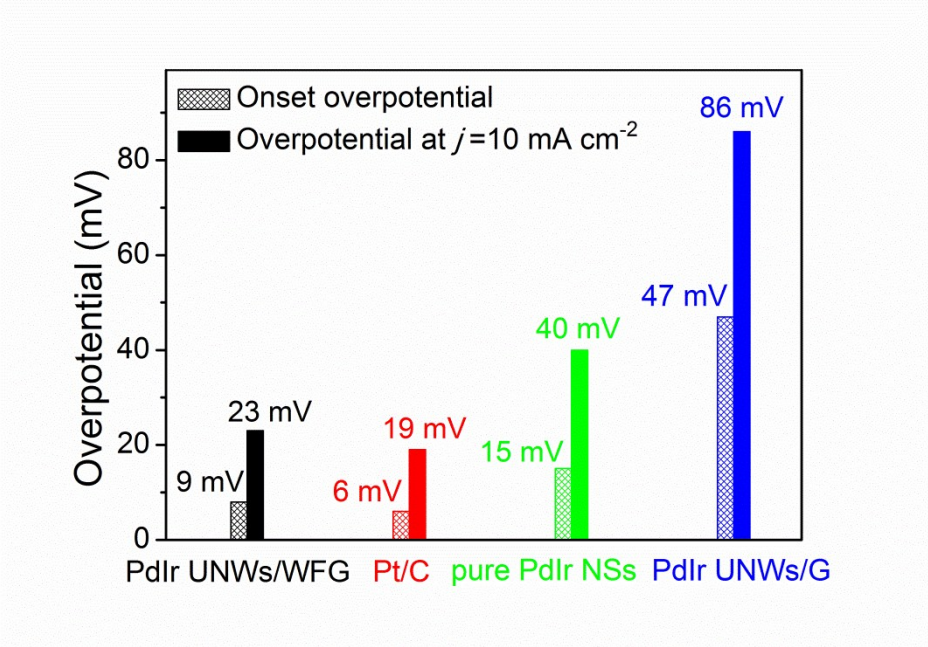

Fig. S8 Histograms of HER onset overpotentials and overpotentials to achieve a current density of 10 mA cm^{-2} for different electrocatalysts.

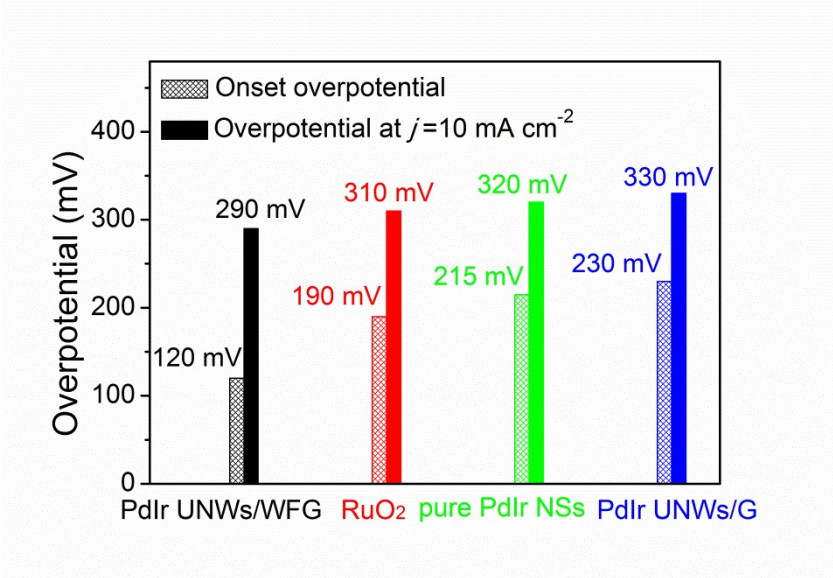

Fig. S9 Histograms of OER onset overpotentials and overpotentials to achieve a current density of 10 mA cm^{-2} for different electrocatalysts.

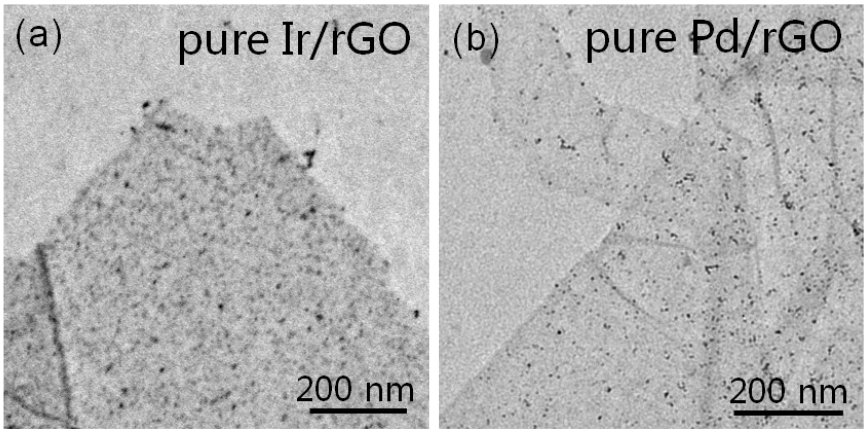

Fig. S10 Representative TEM images of (a) pure Ir/rGO nanocomposites, (b) pure Pd/rGO nanocomposites.

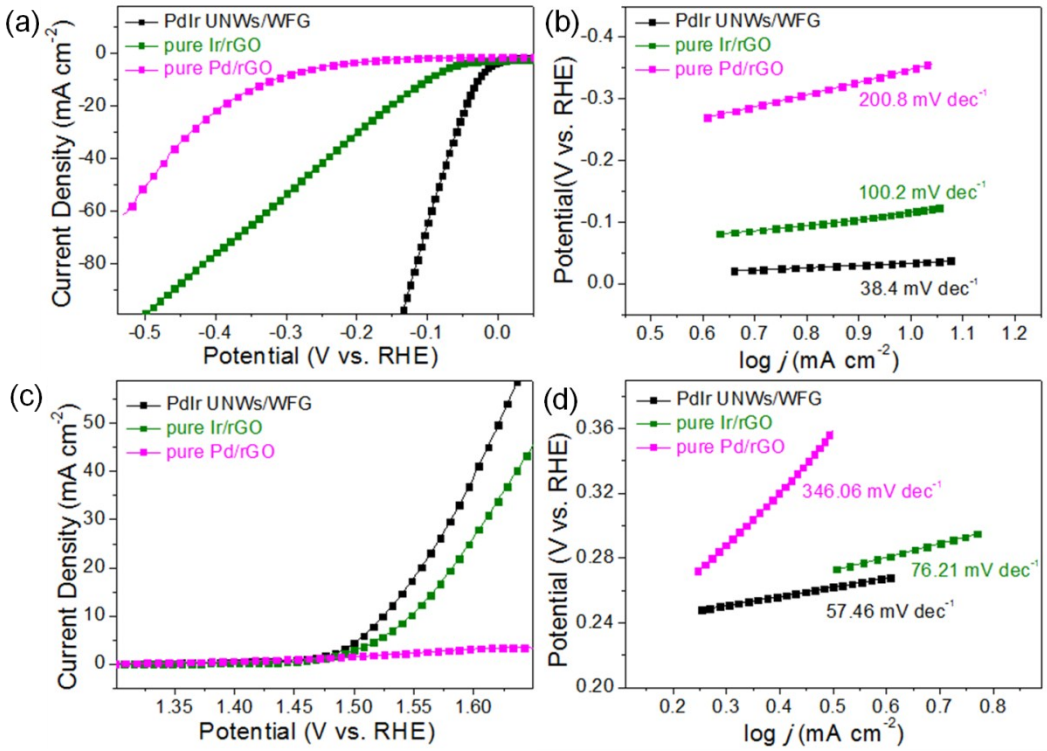

Fig. S11 (a) HER linear sweep voltammetry curves of PdIr UNWs/WFG, pure Ir/rGO, and pure Pd/rGO, respectively. (b) Tafel plots of PdIr UNWs/WFG, pure Ir/rGO, and pure Pd/rGO, respectively.. (c) OER linear sweep voltammetry curves of PdIr UNWs/WFG, pure Ir/rGO, and pure Pd/rGO, respectively.. (d) Tafel plots of of PdIr UNWs/WFG, pure Ir/rGO, and pure Pd/rGO, respectively. All of the above electrolytes are 1.0 M KOH solution.

Table S1. Comparison of the HER performance of the synthesized PdIr UNWs/WFG with some previously reported efficient catalysts in KOH solution.

Catalyst	η*j*=10·mA cm^{-2} /mV	Tafel slope /mV dec^{-1}	Reference
PdIr UNWs /WFG	23	38.4	This work
$Co(OH)_2$-Au-$Ni(OH)_2$	200	92	*Adv. Funct. Mater*. **2018**, 28, 1804361
Ir/MoS_2	44	32	*ACS Energ. Lett.* **2019**, 4, 368−374
Rh nanocrystals	43	107.2	*ACS Appl. Mater. Interfaces* **2016**, 8, 4718-4723
PdP_2@CB	35.4	42.1	*Angew. Chem. Int. Ed.* **2018**, 57, 14862-14867
$Ir_{0.80}Ru_{0.20}O_y$	35	31.5	*ACS Appl. Mater. Interfaces* **2018**, 10, 541-549
Pd@Ru nanorods	30	30	*ACS Appl. Mater. Interfaces* **2018**, 10, 34147-34152
Ru/C_3N_4/C	79	60	*Adv. Funct. Mater.* **2017**, 27, 1606635
Pd-Pt	71	31	*ACS Appl. Mater. Interfaces* **2017**, 9, 18008-18014
β-$Ni(OH)_2$/Pt	92	42	*ACS Energy Lett.* **2018**, 3, 237-244
Pt/NiO@Ni/NF	34	39	*ACS Catal.* **2018**, 8, 8866-8872

Table S2. Comparison of the OER performance of the synthesized PdIr UNWs/WFG with some previously reported efficient catalysts in KOH solution.

Catalyst	η*j*=10 mA cm^{-2} /mV	Tafel slope /mV dec^{-1}	Reference
PdIr UNWs /WFG	290	57.5	This work
$Co(OH)_2$-Au-$Ni(OH)_2$	340	40	*Adv. Funct. Mater.* **2018**, 28, 1804361
Ir/MoS_2	330	44	*ACS Energ. Lett.* **2019**, 4, 368-374
Rh nanocrystals	360	87	*ACS Appl. Mater. Interfaces* **2016**, 8, 4718-4723
$NdBaMn_2O_{5.5}$	430	75	*ACS Catal.* **2018**, 8, 364-371
PdP_2@CB	270	78.6	*Angew. Chem. Int. Ed.* **2018**, 57, 14862-14867
$Ni_{2/3}Fe_{1/3}$-rGO	210	40	*ACS Nano* **2015**, 9, 2, 1977-1984
IrO_x	480	105	*J. Phys. Chem. C* **2018**, 122, 12207-12214
$Ir_{0.46}Co_{0.54}O$	310	58.6	*ACS Appl. Mater. Interfaces* **2017**, 9, 35057-35066
Fe_2O_3/Pd	383	49	*ACS Catal.* **2018**, 8, 6617-6626
Mn/Ru	260	65	*ACS Catal.* **2016**, 6, 2408-2415

Table S3. Comparison of the water splitting performance of the synthesized PdIr UNWs/WFG with some previously reported efficient catalysts in KOH solution.

Catalyst	$\eta^{*}j$=10 mA cm^{-2} /V	Reference
PdIr UNWs /WFG	1.51	This work
$Co(OH)_2$-Au-$Ni(OH)_2$	1.75	*Adv. Funct. Mater.* **2018**, 28, 1804361
Ir/MoS_2	1.57	*ACS Energ. Lett.* **2019**, 4, 368-374
$NdBaMn_2O_{5.5}$	1.65	*ACS Catal.* **2018**, 8, 364-371
PdP_2@CB	1.59	*Angew. Chem. Int. Ed.* **2018**, 57, 14862-14867
Ru_2Ni_2 SNs/C	1.58	*Nano Energy,* **2018**, 47, 1-7
Co–Pt/C	1.54	*J. Mater. Chem. A,* **2018**, 6, 20214-20223
Ni_3FeN/r-GO	1.60	*ACS Nano,* **2018**, 12, 245-253